

Hydrothermal Synthesis of Dy Doped TiO₂(B) Nanowires

Korrakot Pauekphong ^{a,*}, Kalayanee Kooptarnond ^a, Matthana Khangkhamano ^a,
Mahamasuhaimi Masae ^b

^a Department of Mining and Materials Engineering, Faculty of Engineering, Prince of Songkla University, Hat Yai, 90112 Thailand

^b Department of Industrial Technology, Faculty of Engineering, Rajamangala University of Technology Srivijaya, Songkhla, 90000 Thailand

Received 1 February 2019; Revised 5 April 2019; Accepted 19 April 2019

Abstract

This study aimed to synthesize and then characterize the physical property of dysprosium doped TiO₂(B) nanowires powders (Dy/TiO₂(B) NWs). This composite was prepared by hydrothermal method. Phase formation of TiO₂ was characterized by XRD. Morphology of the TiO₂ nanowires powders (NWs) was observed by using field emission scanning electron microscope (FESEM). Optical absorption of the composite had been measured employing UV-Vis spectrophotometer. The result of the physical properties showed a smaller size of Dy/TiO₂(B) NWs crystal 13.8 nm than of TiO₂(B) crystal 20.7 nm by the x-ray diffraction test. Only the TiO₂(B) phase was found at the calcination temperature of 400 °C. The 0.1 mole% dysprosium has good electrical properties. The expected overall properties of Dy/TiO₂(B) NWs may open the way towards new applications of high-performance materials, leading to an innovative product development in the solar cell, electronics batteries and many other applications.

KEYWORDS: TiO₂(B) phase nanowire; Hydrothermal; Dysprosium (Dy)

*Corresponding authors; e-mail: korrakot-p@hotmail.com

Introduction

TiO₂ is a semiconductor material used widely for studies due to photochemical stability, electronic properties, high photocatalytic activity, non-toxicity and low cost. However, applications of TiO₂ are used in energy as an excitation source. In general, TiO₂ has 4 crystal forms, anatase, rutile, brookite, and monoclinic TiO₂(B) structure. TiO₂(B) structure has been higher voids oxygen vacancies and lower density [1 – 5]. TiO₂ can be synthesized using the application of several procedures, such as chemical vapor deposition (CVD) [6], sol-gel [7, 8], microwave [9], electrospinning [10, 11] and hydrothermal [8, 12, 13].

Rare earth (RE) metal ions are usually employed by the researchers as catalyst for the incompletely occupied 4f and empty 5d orbitals [14]. Some experimental results have indicated that the photocatalytic activity of TiO₂ could be promoted by the modification of RE metals [15]. Among the lanthanide series, the Dy doped materials have attracted much attention due to their white light emission. Based on the host environment, Dysprosium has a single oxidation state (Dy³⁺), the 4f electrons give dysprosium an advantage for various functional luminescence

applications. Dysprosium's fluorescence spectrum subsists of numerous traces that are observed, especially in the 470 – 500 nm and 570 – 600 nm regions in host lattices. Alternative, TiO₂, a well-known huge band gap semiconductor [16, 17], has confirmed the possibility to be a good sensitizer to take in light and transfer energy to RE ions [18]. Therefore, the fabrication of structurally pure, concentration managed, TiO₂:RE nanostructures with an emission conduct is still a challenging project for their utilization in optoelectronics [19].

To date, dysprosium doped TiO₂(B) composites have been investigated; however, to our knowledge, there have been no reports regarding the Dy doped TiO₂(B) composites nanowire (NWs) particularly by novel hydrothermal method. Hydrothermal is a method involving a wet chemical process with relatively low temperature and autogenously pressure. This has the advantage of ease of controlling the synthesis process, low energy consumption, cost-effectiveness, and is environmentally safe.

In this paper, synthesis of Dy/TiO₂(B) NWs by hydrothermal method and characterized will be reported in detail. Crystallization,

microstructure and optical properties of the powders were characterized. The photocatalytic properties of the Dy/TiO₂(B) NWs were investigated. Also, the mechanism for improving the photocatalyst activity and electrical property was discussed.

Materials and Methods

Synthesis of Dy/TiO₂(B) NWs by hydrothermal method

In a typical preparation procedure, Degussa P25 TiO₂ nano powder mixed with 30 mL of 10 M sodium hydroxide (NaOH, 98%, Lobachemie) and Dysprosium Nitrate (DyN₃O₉, 99.9%, Sigma-Aldrich) corresponding to different Dy/Ti proportioning of (0 and 0.1 at mol.%) were sonicated for 60 minutes in an ultrasonic. The mixture was transferred to a 50 mL teflon-lined autoclave container and heated at 220 °C for 24 h. After cooling to room temperature, the mixtures were taken out, and then were rinsed extensively with 0.1 M HCl, deionized water and subsequently with ethanol. Then, the mixture was annealed at 400 °C for 2 h.

Characterization of TiO₂(B) NWs

The X-ray diffraction (XRD) patterns were characterized in terms of phase compositions and crystallite size by using an X-ray diffractometer (Phillips E'pert MPD, CuK_α). The surface morphology of the prepared powders was characterized by field emission scanning electron microscope (FESEM, Apreo, FEI). The band gap energy value of TiO₂ in the powder form UV-vis absorption spectra were obtained by UV-vis spectrophotometer (UV-2401, Shimadzu by using BaSO₄ as reference). The study of DC electrical conductivity property of powder samples used an LCR-meter (Agilent 4285A Precision) in the frequency test range 75 kHz – 30 MHz, with 100 Hz steps at room temperature.

Results and Discussion

XRD Analysis

The XRD patterns of TiO₂ powders calcined at 400 °C by hydrothermal method are presented

in Fig. 1. It was found that only the TiO₂(B) phase can be seen at 0 and 0.1 mol.% Dy doping in TiO₂. The diffraction peaks which appear in undoped TiO₂ sample at 2θ are 14.18, 25.32, 29.26, 44.39 and 48.29 respectively. According to the JCPDS 46-1238 patterns of TiO₂(B) phase form TiO₂ monoclinic structure requirements and no found position of Dy. The crystallite size was determined from XRD peaks using the Scherrer equation (1) [20],

$$D = 0.9\lambda / \beta \cos \theta \quad (1)$$

where D is the crystalline size (nm), λ is the wavelength of the X-ray radiation (CuK_α = 0.15406nm), β is the angle width at half maximum height, and θ is the half diffraction angle in degree of the centroid of the peak. The Dy doping seems to affect the crystal phase from the Scherrer formula, the average crystallite sizes of Dy/TiO₂(B) NWs are estimated to be about 13.8 nm (Table 1), Dysprosium retards the grain size. In addition, lattice parameter of TiO₂ can be calculated from XRD patterns [11], The difference in lattice constant suggests that Dy³⁺ ions are doped in to the crystal lattice of TiO₂ [21]. However, there is a distinction between the lattice parameters of the pure TiO₂ and Dy/TiO₂(B) NWs, which may be due to the formation of stresses by the difference in ionic size between Ti (~0.6 Å) and Dy (~0.91 Å) (Table 1) [22, 23], which cause the increase of the unit cell.

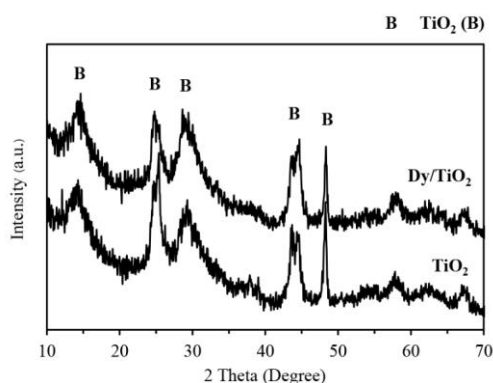


Fig.1 XRD patterns of pure TiO₂ NWs and Dy/TiO₂(B) NWs calcined at 400 °C.

Table 1 Crystallite size, Lattice parameters and Volume of cell of pure TiO₂ and Dy/TiO₂(B) NWs.

Sample	Crystalline size (nm)	Lattice parameters (Å)				Volume of cell (Å ³)
		a	b	c	β	
TiO ₂ NWs	20.7	12.20	3.75	6.53	107.36°	286.13
Dy/TiO ₂ NWs	13.8	13.44	3.76	6.56	107.36°	316.40

Morphology of Dy/TiO₂(B) NWs

Morphology of the Dy/TiO₂(B) NWs prepared by hydrothermal method for 24 h at 220 °C and calcined 400 °C was observed by FESEM illustrated in Fig. 2. It can be seen that Dy/TiO₂(B) NWs nucleated are homogeneous. The average diameter and length of Dy/TiO₂(B) NWs are about 86.3 – 251.2 nm and 0.6 – 5.1 μm, respectively.

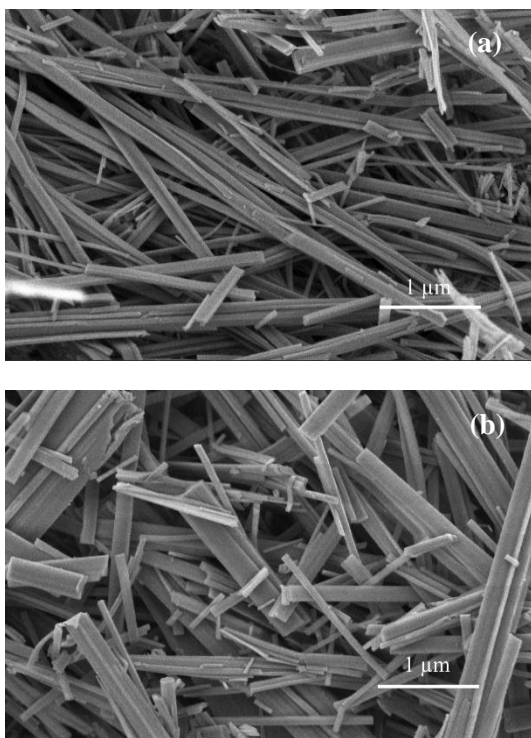


Fig. 2 FESEM images of (a) pure TiO₂ NWs and (b) Dy/TiO₂(B) NWs

Energy gap measurement

The UV-vis spectra of TiO₂(B) NWs and Dy/TiO₂(B) NWs are shown in Fig. 3a. The band gap energies (E_g) of the samples was determined and analyzed by intercept x of the linear portion of $(\alpha h\nu)^2$ as a function of E to $\alpha E = 0$ (where $E = E_g$)

of following equation (2) [24],

$$\alpha E = A'(E - E_g)^m \quad (2)$$

where E_g is the band gap energy (eV) of the sample and λ is the wavelength of the on set of the spectrum (nm). ($E = hc/\lambda$), respectively. $M = 1/2$ for direct band gap and $m = 2$ for indirect band gap. The absorption coefficient (α) was calculated by $\alpha = A/d'$ where A is the measured absorbance (nm), d' is the thickness of samples in UV-vis cell (0.4 cm).

Figure 3(b) shows the direct band gap of the pure TiO₂ NWs is 3.44 eV [8]. It is decreased to 3.39 eV with the addition of dopant Dy³⁺. Decrease in the optical band gap of the nanostructure observed can be attributed to the reduction of the crystallite size. The optical band gap shift of Dy/TiO₂ NWs from the optical band gap of pure TiO₂ NWs indicates the red shift. Furthermore, since Dy doping causes narrower band gap energy of the photocatalyst as depicted in Fig 3, formations of electron-hole pairs on the photocatalyst surface also increase, resulting in the highest photocatalytic activity because the absorption wavelength range is towards visible light and hence the increase in absorption intensity. From the results, it is ascertained that photocatalytic activity of Dy/TiO₂ NWs photocatalyst is strongly dependent on the amount of doped Dy concentration [25, 26]. This effect of Dy doping in TiO₂ on enhancement of visible light absorption capacity agrees well with the previous works [13]. In addition we discuss the probable reason of band gap narrowing in TiO₂ with Dy doping in hydrothermal treatment. As reported, the Dy dopant acts as an acceptor impurity in TiO₂ lattice [13]. Thus when the TiO₂ is doped with Dy, the acceptor levels of Dy along with oxygen vacancies are created in the band gap of TiO₂. In our case, as discussed above Ti³⁺ is also formed which creates energy level in the band gap, contributing to the reduction of band gap (Table 2).

Table 2 Band gap energy and Oxygen vacancy of samples

Sample	Band gap energy (eV.)	Oxygen vacancy
TiO ₂ NWs	3.44	2.76
Dy/TiO ₂ NWs	3.39	2.91

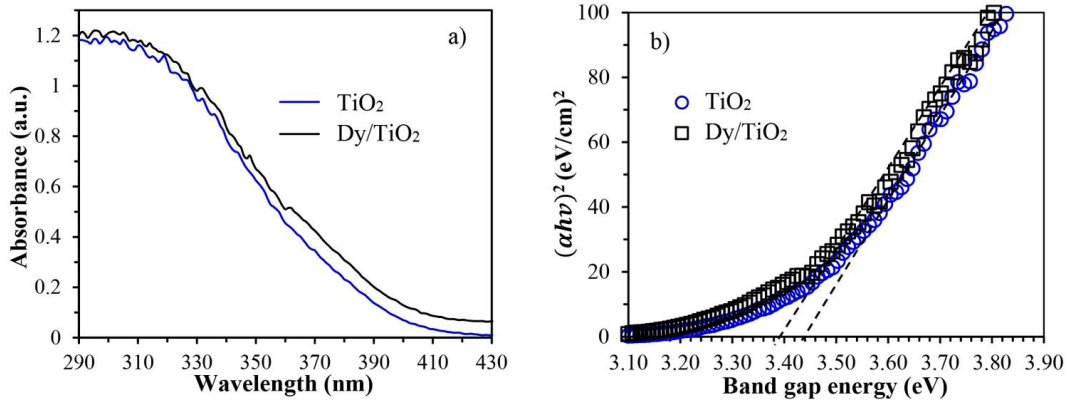


Fig. 3 (a) UV-vis spectra and (b) evolution of $(\alpha h\nu)^2$ versus photon energy curves of pure TiO₂ NWs and Dy/TiO₂ NWs calcined at 400 °C for 2 h.

Electrical properties

The DC electrical conductivity and dielectric loss of nanocomposite Dy/TiO₂ sample powder using LCR-meter in the range frequency test 75kHz – 30MHz at room temperatures can be calculated by the following equation (3) and (4) [27],

$$\sigma_{DC} = 1 / \rho_{DC} = (1 / R) \cdot (L / A) \quad (3)$$

where σ_{DC} is the DC conductivity, ρ_{DC} is the resistivity of the sample, R is the resistance, L is the thickness and A is the area of the samples.

$$\varepsilon'' = 1 / 2\pi F \cdot C_p \cdot R_p \quad (4)$$

where ε'' is dielectric loss, F is the frequency, C_p is the capacitance in parallel and R_p is the resistance in parallel.

As shown in Fig. 4, DC electrical conductivity increases with the increasing of frequency. At higher frequency range, a higher DC conductivity of the material also increases as hopping frequency of the free electrons is accelerated [28]. The DC conductivity at high frequencies is the trend required for a small polaron hopping [29 – 31]. For the host nanomaterials, conductivity exhibited with fairly localized vendors bound to the lattice with lattice strain i.e. with polaron conduction [29, 32, 33]. It is seen that with addition of Dy, conductivity value increases in the high frequency. The Dy addition may result in more localization of charge carriers along with mobile ions causing higher ionic conductivity because the Dy dopant acts as an acceptor impurity in TiO₂ lattice and an inhibition of the recombination of electron–hole pairs. Moreover, the defect concentration or oxygen vacancy concentration around grain boundaries strongly affects the motion of charge carriers suggesting the performance in electrical

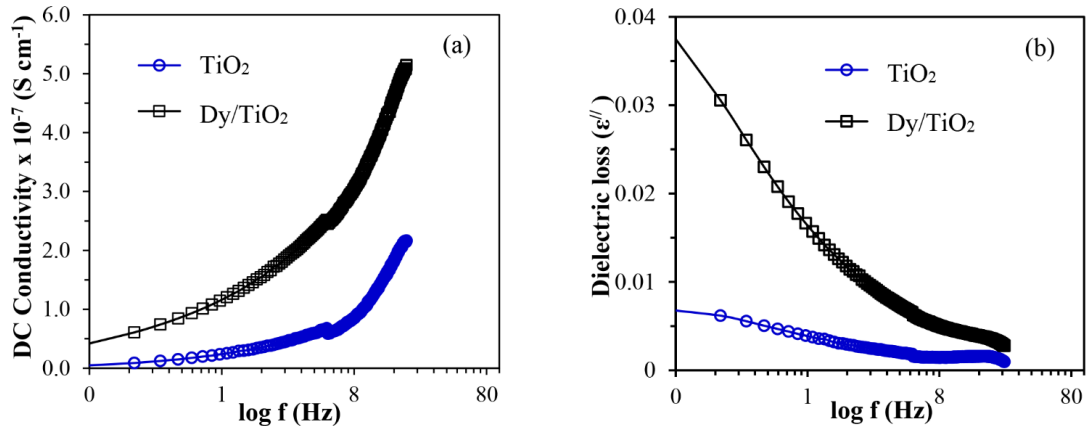


Fig. 4 Electrical properties of pure TiO₂ and Dy/TiO₂ NWs (a) DC Conductivity and (b) Dielectric loss

conductivity. This may be the reason for higher conductivity and strong frequency dispersion on Dy [13, 34]. As expected, the conductivity increases with doped Dy. The conductivity of Dy/TiO₂ NWs was increased by 0.42×10^{-7} S cm⁻¹ relative to 0.05×10^{-7} S cm⁻¹ for pure TiO₂ NWs. The Dy crystal dispersion of TiO₂(B) phase particles is due to the phase action of Dy/TiO₂ NWs. It helps in controlling the internal individual dipoles in the presence of electric field and hence, controls the conductivity properties of the composite.

Conclusion

We have successfully fabricated single crystalline Dy/TiO₂ NWs using the hydrothermal process. This method produced a large quantity of single crystalline NWs at relatively high purity and very low cost. The Dy/TiO₂ NWs have very strong electrical properties. The Dy/TiO₂ NWs may have many potential applications in photocatalysts and photoelectronics.

Acknowledgements

The authors would like to acknowledge the Department of Mining and Materials Engineering, the Faculty of Engineering, the Graduate School, Prince of Songkla University (PSU), Thailand for financial support of this research.

References

- [1] A. Fujishima, K. Honda, Electrochemical Photolysis of Water at a Semiconductor Electrode, *Nature*. 238 (1972) 37 – 38.
- [2] D.V. Bavykin, A.A. Lapkin, P.K. Plucinski, J.M. Friedrich, F.C. Walsh, TiO₂ Nanotube-Supported Ruthenium(II) Hydrated Oxide: A Highly Active Catalyst for Selective Oxidation of Alcohols by Oxygen, *J. Catal.* 235 (2005) 10 – 17.
- [3] X. Chen, S.S. Mao, Titanium Dioxide Nanomaterials: Synthesis, Properties, Modifications and Applications, *Chem. Rev.* 107 (2007) 2891 – 2959.
- [4] J.H. Park, S. Kim, A.J. Bard, Novel Carbon-Doped TiO₂ Nanotube Arrays with High Aspect Ratios for Efficient Solar Water Splitting, *Nano Lett.* 6 (2006) 24 – 28.
- [5] S.K. Mohapatra, M. Misra, V.K. Mahajan, K.S. Raja, A Novel Method for the Synthesis of Titania Nanotubes Using Sono-electrochemical Method and Its Application for Photoelectrochemical Splitting of Water, *J. Catal.* 246 (2007) 362 – 369.
- [6] S. Feng, J. Yang, M. Liu, H. Zhu, J. Zhang, G. Li, J. Peng, Q. Liu, CdS Quantum Dots Sensitized TiO₂ Nanorod-Array-Film Photoelectrode on FTO Substrate by Electrochemical Atomic Layer Epitaxy Method, *Electrochim. Acta.* 83 (2012) 321 – 326.
- [7] A. Sadeghzadeh Attar, M. Sasani Ghamsari, F. Hajiesmaeilbaigi, Sh. Mirdamadi, K. Katagiri, K. Koumoto, Sol-Gel Template Synthesis and Characterization of Aligned Anatase-TiO₂ Nanorod Arrays with Different Diameter, *Mater. Chem. Phys.* 113 (2009) 856 – 860.
- [8] Valencia, Sergio, Juan Miguel Marín, and Gloria Restrepo, Study of the Bandgap of Synthesized Titanium Dioxide Nanoparticles Using the Sol-Gel Method and a Hydrothermal Treatment, *Open Mater. Sci. J.* 4 (2009) 9 – 14.
- [9] L. Li, X. Qin, G. Wang, L. Qi, G. Du, Z. Hu, Synthesis of Anatase TiO₂ Nanowires by Modifying TiO₂ Nanoparticles Using the Microwave Heating Method, *Appl. Surf. Sci.* 257 (2011) 8006 – 8012.
- [10] J.S. Lee, Y.I. Lee, H. Song, D.H. Jang, Y.H. Choa, Synthesis and Characterization of TiO₂ Nanowires with Controlled Porosity and Microstructure Using Electrospinning Method, *Curr. Appl. Phys.* 11 (2011) S210 – S214.
- [11] P.S. Archana, R. Jose, T.M. Jin, C. Vijila, M.M. Yusoff, S. Ramakrishna, Structural and Electrical Properties of Nb-Doped Anatase TiO₂ Nanowires by Electrospinning, *J. Am. Ceram. Soc.* 93 (2010) 4096 – 4102.
- [12] A. Fujishima, T.N. Rao, D.A. Tryk, Titanium Dioxide Photocatalysis, *J. Photochem. Photobiol. C* 1 (2000) 1 – 21.
- [13] S.E. Arasi, M.V.A. Raj, J. Madhavan, Impact of Dysprosium (Dy³⁺) Doping on Size, Optical and Dielectric Properties of Titanium Dioxide Nanoparticles Grown by Low Temperature Hydrothermal Method, *J. Mater. Sci-Mater El.* 29 (4) (2018) 3170 – 3177.
- [14] P. Yang, C. Lu, N. Hua, Y. Du, Titanium Dioxide Nanoparticles Co-Doped with Fe³⁺ and Eu³⁺ Ions for Photocatalysis, *Mater. Lett.* 57 (2002) 794 – 801.
- [15] A. W. Xu, Y. Gao, H.Q. Liu, The Preparation, Characterization, and Their Photocatalytic Activities of Rare-Earth-Doped TiO₂ Nanoparticles, *J. Catal.* 207 (2002) 151 – 157.
- [16] G. Wakefield, E. Holland, P.J. Dobson, J.L. Hutchison, Luminescence Properties of Nanocrystalline Y₂O₃: Eu, *Adv. Mater.* 13 (2001) 1557 – 1560.

- [17] L. Wang, Y. Li, Na(Y_{1.5}Na_{0.5})F₆ Single-Crystal Nanorods as Multicolor Luminescent Materials, *Nano Lett.* 6 (2006) 1645 – 1649.
- [18] F. Zhang, N. Huang, P. Yang, X. Zeng, Y. Mao, Z. Zheng, Z. Zhou, X. Liu, Blood Compatibility of Titanium Oxide Prepared by Ion-Beam-Enhanced Deposition, *Surf. Coat. Tech.* 84 (1996) 476 – 479.
- [19] On the Construction and Practice of Cubic Practical Teaching System for It Applied Personnel Cultivating. WIT Transactions on Information and Communication Technologies. 2014.
- [20] H.L. Qin, G.B. Gu, S. Liu, Preparation of Nitrogen-Doped Titania with Visible-Light Activity and Its Application, *CR. Chim.* 11 (2008) 95 – 100.
- [21] J.Y. Kuang, Y.L. Liu, Trapping Effects in CdsiO₃:In³⁺ Long Afterglow Phosphor, *Chinese Phys. Lett.* 23 (2006) 204 – 206.
- [22] A. Khataee, R.D.C. Soltani, Y. Hanifehpour, M. Safarpour, H.G. Ranjbar, S.W. Joo, Synthesis and Characterization of Dysprosium-Doped ZnO Nanoparticles for Photocatalysis of a Textile Dye under Visible Light Irradiation, *Ind. Eng. Chem. Res.* 53 (2014) 1924 – 1932.
- [23] E.J. Lee, J. Jeong, Y.H. Han, Electrical Properties of Dy₂O₃-Doped BaTiO₃, *Jpn. J. Appl. Phys.* 43 (2004) 8126 – 8129.
- [24] B. Xu, J. Ding, L. Feng, Y. Ding, F. Ge, Z. Cai, Self-Cleaning Cotton Fabrics Via Combination of Photocatalytic TiO₂ and Superhydrophobic SiO₂, *Surf. Coat. Tech.* 262 (2015) 70 – 76.
- [25] J. Dhanalakshmi, D.P. Padiyan, Corroboration of Structural Properties of Dy₂O₃-TiO₂ Nanocomposites through X-Ray Diffraction and Raman Spectroscopy, *Nano Hybrids Comp.* 17 (2017) 127 – 130.
- [26] M. Zikriya, Y.F. Nadaf, C.G. Renuka, Morphological and Structural Characterization of Dy³⁺ Doped Titanium Dioxide, *Mater. Today- Proc.* 5 (2018) 10805 – 10813.
- [27] N. Sriharan, N. Muthukumarasamy, T.S. Senthil, Preparation and Characterization of Al₂O₃ Doped TiO₂ Nanocomposites Prepared from Simple Sol-Gel Method, *Z. Phys. Chem.* 230 (2016) 1745 – 1758.
- [28] R. Chang, Y. Tian, Y. Wang, J. Qin, Ph-Responsive Vesicles with Tunable Membrane Permeability and Hydrodynamic Diameters from a Cross-Linkable Amphiphilic Block Copolymer, *Nanomater Nanotechno.* 6 (2016) 6.
- [29] S. Sagadevan, K. Pal, P. Koteeswari, A. Subashini, Synthesis and Characterization of TiO₂/Graphene Oxide Nanocomposite, *J. Mater. Sci-Mater. El.* 28 (2017) 7892 – 7898.
- [30] A.N. Patil, M.G. Patil, K.K. Patankar, V.L. Mathe, R.P. Mahajan, S.A. Patil, Dielectric Behaviour and Ac Conductivity in Cu_xFe_{3-x}O₄ Ferrite, *B. Mater. Sci.* 23 (2000) 447 – 452.
- [31] S. Kurian, S. Sebastian, J. Mathew, K.C. George, “Structural and Electrical Properties of Nano-Sized Magnesium Aluminate,” *Indian J. Pure. Ap. Phy.* 42(12) (2004) 926 – 933.
- [32] C.R. Indulal, R. Raveendran, Synthesis, Characterization and Dielectric Studies of Cerium Phospho Iodate and Cadmium Doped Cerium Phospho Iodate in Nano Form, *Indian J. Pure. Ap. Phy.* 48(2) (2010) 121 – 126.
- [33] M. Raghasudha, D. Ravinder, P. Veerasomaiah, Influence of Cr³⁺ Ion on the Dielectric Properties of Nano Crystalline Mg-Ferrites Synthesized by Citrate-Gel Method, *Mater. Sci. Appl.* 4 (2013) 432 – 438.
- [34] D. Roy, P. Sultana, S. Ghosh, S. Das, P. Nandy. Electrical and Dielectric Properties of TiO₂ and Fe₂O₃ Doped Fly Ash, *Bull. Mater. Sci.* 36(7) (2013) 1225 – 1230.